PAPER

Silanization effect on the photoluminescence characteristics of crystalline and amorphous silicon nanoparticles†

Paula Caregnato,* Maria Laura Dell'Arciprete and Mónica Cristina Gonzalez

Silicon nanoparticles synthesized by two different methods were surface modified with 3-mercaptopropyltrimethoxysilane. The particles of ~2 nm size exhibit photoluminescence (PL) in the UV-Vis range of the spectrum. The most intense PL band at 430 nm with an emission lifetime of 1–2 ns is attributed to the presence of the surface defects Si–O–Si, generated after anchoring the organic molecule onto the interface. The excitation–emission matrix of this band is essentially independent of the technique of synthesis, crystalline structure, and size of the silicon nanoparticles.

1. Introduction

The desirability of constructing optoelectronic and fluorescence display devices and sensors[1,2] based on silicon has prompted the exponentially growing interest in the preparation and characterization of light-emitting silicon nanomaterials.[3]

Silicon is a common trace element in humans and the primary biodegradation product of porous Si, orthosilicic acid ($Si(OH)_4$), is the form predominantly absorbed by humans and is naturally present in numerous tissues.[4,5] Nanoparticles and porous silicon have low toxicity, and most importantly, they are biodegradable and biocompatible.[6,7]

Silicon nanoparticles of radii smaller than 4 nm have an effect of quantum confinement imposed upon the charge carriers.[8] These particles received great attention, because besides being photosensitizers of singlet oxygen, they combine size-dependent photoluminescence with the richness of silicon surface chemistry.[9,10]

It is known that organosilane 3-mercaptopropyltrimethoxysilane (MPTS), commonly used as a silanization reagent, can be quickly chemisorbed onto the surfaces of silicon materials containing –OH groups *via* strong covalent Si–O–Si bonds with terminal thiol groups.[11] The pendant–SH groups are useful in surface modification strategies owing to their diversified reactions. For example, nanoparticles used for drug and gene delivery, where thiol groups are used as linkers for binding biomolecules (with other thiol groups forming disulfide bonds with the target molecule).[12] Besides, owing to its strong affinity to noble metals such as Au, pendant thiol can be used to capture Au nano-particles in colloidal solutions.

Thiol groups attached to nanoparticles may not be inert to oxidative stress reactions. It was previously reported that thiols supported on a silica matrix is a clean source of thiyl radicals, which would be useful to simulate nondiffusional reactions involved in thiol/thiyl radicals attached to macromolecules.[13]

Here, we report the synthesis of silicon nanoparticles by two different approaches: treated porous silicon colloids (PSi-NP) and bottom-up silicon nanoparticles (Si-NP). These particles were further modified by a silanization reaction with 3-mercaptopropyltrimethoxysilane, obtaining PSi-NP-SH and Si-NP-SH nanoparticles.

Morphology and surface chemistry were studied by Transmission Electron Microscopy (TEM), Scanning Tunneling Microscopy (STM), Atomic Force Microscopy (AFM), Fourier Transformed Infrared Spectroscopy (FTIR), Raman spectroscopy and X-ray Photoelectron Spectroscopy (XPS).

Steady-state and time-resolved luminescence, as well as time-domain anisotropy, measurements were performed, to study the effect on PL of the introduction of surface siloxane bonds as a result of silanization.

2. Results and discussion

Sample characterization

Transmission electron microscope (TEM). Representative TEM images for PSi-NPs shown in Fig. 1 indicate formation of stable aggregates larger than 20 nm, composed of crystalline silicon particles of <5 nm size. The diffraction pattern indicates an essentially crystalline nature for the particles.

Instituto de Investigaciones Fisicoquímicas Teóricas y Aplicadas (INIFTA), Facultad de Ciencias Exactas. Universidad Nacional de la Plata, C.C. 16, suc. 4, (1900) La Plata, Argentina. E-mail: caregnato@inifta.unlp.edu.ar; Fax: +54-221-4254642; Tel: +54-221-4257430
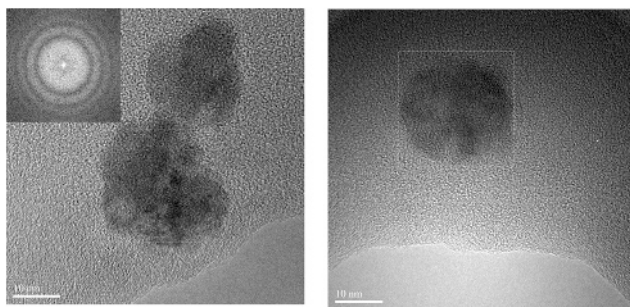†Electronic supplementary information (ESI) available. See DOI: 10.1039/c3pp50067e

1658 | *Photochem. Photobiol. Sci.*, 2013, **12**, 1658–1665

This journal is © The Royal Society of Chemistry and Owner Societies 2013

Fig. 1 HR-TEM images of PSi-NP particles.

Fig. 3 (a) Atomic force microscopy (AFM) image PSi-NP dropcast from toluene dispersion onto a mica substrate. (b) Corresponding histogram of Si nanoparticle heights measured from the AFM image in (a).

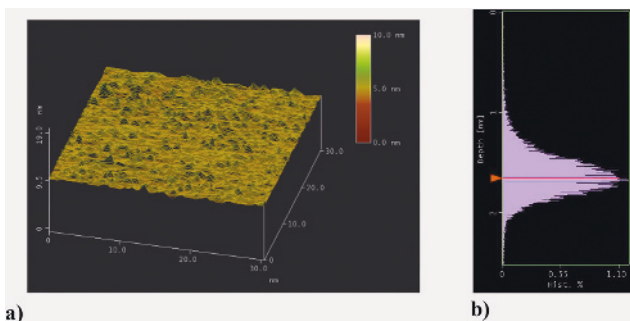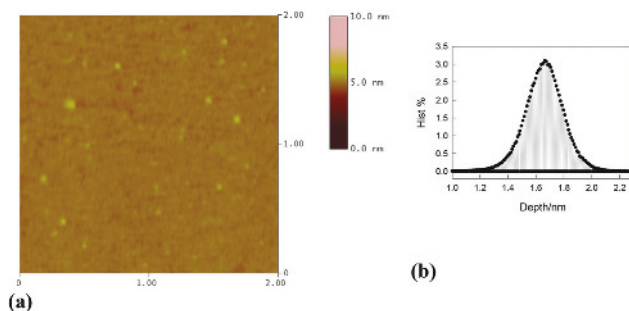**Fig. 2** (a) STM image of PSi-NP-SH on an Au(111) substrate. STM parameters V_{bias}: 100 mV, $I_{set-point}$: 10 nA. (b) Histogram of PSi-NP-SH heights extracted from STM topography.

The average particle diameter of (1.7 ± 0.8) nm of Si-NP nanoparticles was determined by TEM in a previous paper with no evidence of particle crystalline structure.[14]

Scanning tunneling microscope (STM). The topographic STM image of PSi-NP-SH particles anchored on a gold surface *via* Au–S bonds (Fig. 2a) shows well-separated particles that can be easily identified. The size of the particles can be measured in the height profile obtained from the topographic images. In contrast, the lateral dimensions of the nanoparticle are generally larger due to tip convolution effects.[15] Histograms of the height of the particles measured from the topographic images are shown in Fig. 2b. The average STM height is around (1.6 ± 0.5) nm.

For Si-NP-SH the same support was used to chemisorb the nanoparticles, obtaining an STM average height of (0.9 ± 0.2) nm (figure not shown).

Atomic force microscope (AFM). The measurement was performed on PSi-NP samples suspended in toluene, after dropcasting on a mica support and solvent evaporation.

The AFM image is shown in Fig. 3a. From the corresponding AFM histogram, plotted in Fig. 3b, a mean particle height of (1.7 ± 0.3) nm is estimated.

Fourier transform infrared spectra (FTIR). For the PSi-NP-SH sample, the two bands in the range 2937–2838 cm^{-1} are due to aliphatic C–H stretching of the attached thiol propyl groups. The peaks observed at 1074 and 802 cm^{-1} are assigned to the asymmetric and symmetric stretching mode due to vibrational modes of O–Si–O groups, respectively (Fig. 4).[13,16]
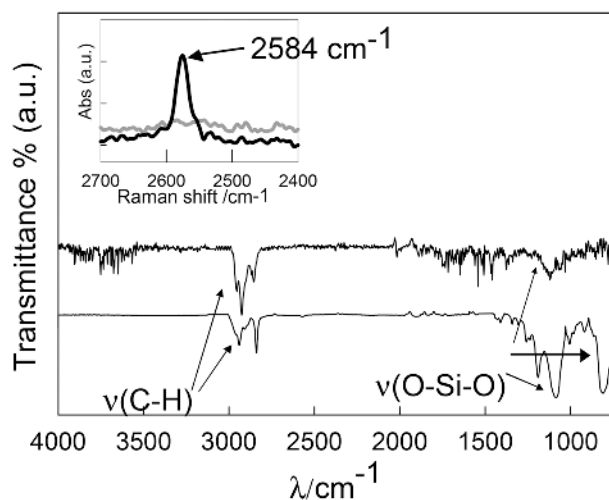
Fig. 4 FTIR spectra of silicon modified nanoparticles: PSi-NP-SH (lower line) and Si-NP-SH (upper line). Inset: FT-Raman spectra in the 2400–2700 cm^{-1} range of bare PSi-NP (grey line) and thiol-modified PSi-NP-SH (black line) silicon nanoparticles.

For Si-NP-SH, the spectrum shows a small absorption peak at 1120 cm^{-1} assigned to O–Si–O vibrations and a small, broad band near 3600 cm^{-1} which corresponds to O–H stretching vibration.[16] The peaks at 2935, 2923 and 2852 cm^{-1} are assigned to the attached thiol propyl groups. However, the presence of surface-adsorbed TOAB used during the synthesis procedure cannot be discarded.[14,17]

Raman spectroscopy. The (C)–S–H stretching vibration (2600–2550 cm^{-1}) gives rise to a very weak absorption in the infrared spectrum. This bond is highly polarizable, and hence produces stronger spectral activity in the Raman spectrum than the infrared.[16] The inset of Fig. 4 shows the Raman shift at 2584 cm^{-1} for PSi-NP-SH, which is attributed to the stretching vibration of the terminal S–H groups.[18]

X-ray photoelectron spectroscopy (XPS). The spectrum of PSi–NP shows signals due to O(1s), Si(2s) and Si(2p) surface elements. The Si(2p) region (see Fig. 5, main figure) displays the contribution of different environments for the silicon atoms. Peaks at 101.4, 102.8 and 103.6 eV with contributions of 16.2, 3.9 and 68.9%, respectively, were assigned to Si(–O–)$_x$

This journal is © The Royal Society of Chemistry and Owner Societies 2013

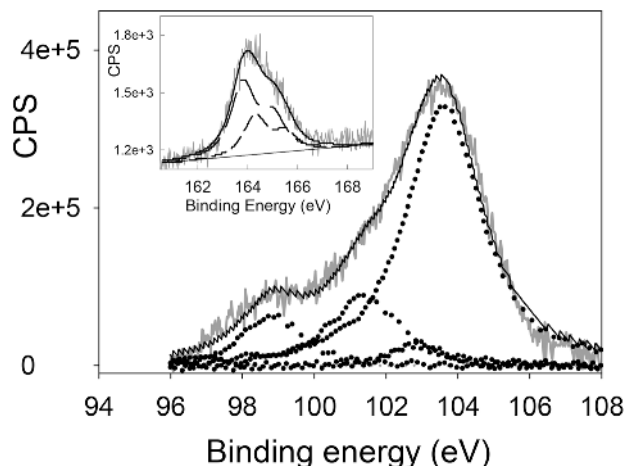*Photochem. Photobiol. Sci.*, 2013, **12**, 1658–1665 | **1659**

Fig. 5 Main: XPS spectrum of the Si(2p) core level of the PSi-NP sample. Inset: XPS spectra of PSi-NP-SH modified silicon nanoparticles in the S(2p) core level region.

coordinated compounds with x = 2, 3, and 4.[18] The peak with a binding energy of 98.8 eV with a contribution of 11.0% is assigned to Si–Si.[19]

The PSi-NP-SH spectrum shows a peak that corresponds to S(2p) at 160–170 eV (see Fig. 5, inset). For each S(2p) doublet, a 1.2 eV spin orbit splitting and a 2 : 1 branching ratio between the 3/2 and 1/2 components was adopted. The peaks within each doublet were assumed to have the same width. The main doublet at 163.8 and 164.3 eV is associated with free thiol (SH) groups.[20,21]

Ratios between the signal areas of the elements corrected for the instrument sensitivity yield a number of two or less silicon atoms per SH group in the PSi-NP-SH suspensions. This means that at least 50% of the oxidized silicon atoms in the surface are silanized after thiol treatment.

Photoluminescence experiments

PSi–NP and Si–NP show PL in the wavelength range from 250 to 600 nm, with the emission spectrum strongly depending on the excitation wavelength in the specified range (see ESI,

Fig. 1,† for the excitation–emission matrix). The dependence of the emission spectrum on the excitation wavelength indicates the contribution of different emitters due to the different particle sizes, agglomeration, oxidation grade and molecules adsorbed on the surface.[14] Therefore, a bilinear regression analysis of the emission–excitation matrix was performed to retrieve the number of species and contribution to the overall excitation–emission matrix. The regression analysis indicates a minimum of three different species contributing to the total emission of the bare surface particles PSi-NP and Si-NP. However, changes in the photoluminescence are observed after surface derivatization, revealing a modification after MPTS anchored silicon surface.

PSi-NP and PSi-NP-SH

Toluene suspensions of PSi-NPs show an excitation–emission maximum at ($\lambda_{exc.}$/nm, $\lambda_{em.}$/nm): (295, 360), (330, 380), and (355, 430), respectively (Fig. 6). These emission contributors were named PSi1, PSi2, and PSi3 according to their excitation–emission maximum.

The graph scales of excitation and emission spectra obtained from bilinear analysis are correlated to show the relative contribution of each species to the overall emission. In Fig. 6 and 7 the intensity was normalized taking the maximum value I = 1.6 for the species PSi1.

Surface-derivatized PSi-NP-SH also show the contribution to the excitation–emission matrix of a minimum of three species, namely PSi-SH1, PSi-SH2 and PSi-SH3 with an excitation–emission maximum at ($\lambda_{exc.}$/nm, $\lambda_{em.}$/nm): (310, 360), (340, 380) and (370, 430), respectively (see Fig. 7 and ESI, Fig. 1,† for the excitation–emission matrix).

The emission traces of toluene suspensions of PSi-NP-SH obtained upon excitation at 341 nm could be well fitted to a bi-exponential function with decay times of (1.40 ± 0.03) and (8.5 ± 0.2) ns. The short-lived component contributes to the emission with a spectrum coincident with those expected for species PSi-SH3, while the long-lived component contribution resembles the emission spectrum of species PSi-SH2, as shown by the symbols in Fig. 7. Excitation at 388 nm yields decay
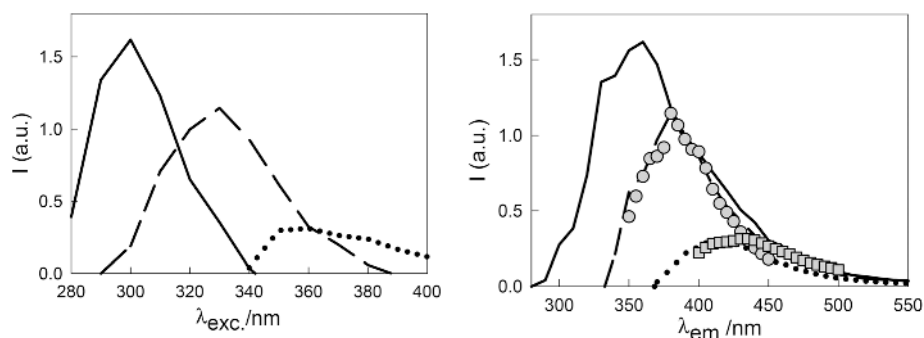

Fig. 6 Normalized excitation (left figure) and emission spectra (right figure) obtained from the bilinear regression analysis of the PSi-NP toluene suspension excitation–emission matrix. The assigned emitting species are PSi1 (solid line), PSi2 (dashed line), and PSi3 (dotted line), respectively. (●) stands for the contribution to the overall emission due to the transient with 8.8 ns decay times observed upon 341 nm. (■) stands for the contribution to the overall emission due to the transients with 3.3 ns decay times, observed upon 388 nm excitation.
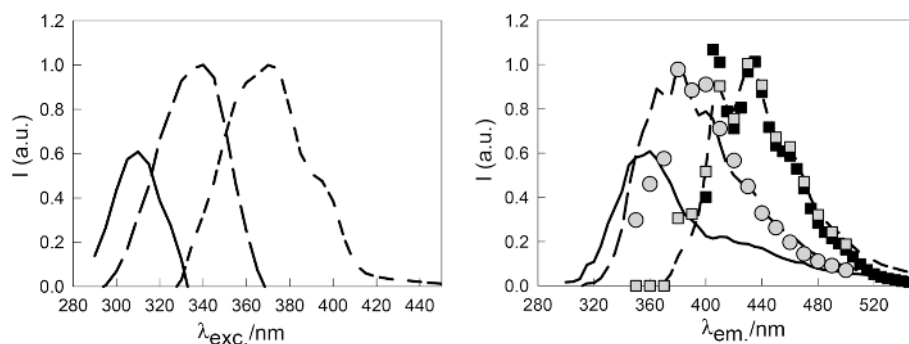
Fig. 7 Normalized excitation (left figure) and emission (right figure) spectrum obtained from the bilinear regression analysis of the PSi-NP-SH toluene suspension excitation–emission matrix. The assigned emitting species are PSi-SH1 (solid line), PSi-SH2 (dashed line), and PSi-SH3 (short dashed line), respectively. (▨) and (●) stand for the contribution to the overall emission due to the transients with 1.4 and 8.5 ns decay times, respectively, observed upon 341 nm excitation. (■) stands for the contribution to the overall emission due to the transients with 1.8 ns decay time, observed upon 388 nm excitation.

signals with a mono-exponential fit of (1.8 ± 0.1) ns decay time and emission spectra with λ_{max} at 435 nm, coincident with that assigned to PSi-SH3 species (see symbols in Fig. 7).

PSi-NP luminescence decays fit to a mono-exponential function with a decay time of (8.8 ± 0.2) ns by exciting at 341 nm. The emission spectrum of this component resembles that obtained for PSi2 by bilinear analysis. Excitation at 388 nm yields decay signals with a mono-exponential fit of (3.3 ± 0.2) ns decay time and emission spectra with λ_{max} at 430 nm, coincident with that assigned to the PSi3 species (see symbols in Fig. 6).

The time-resolved luminescence of PSi1 and PSi-SH1 emitters with negligible contribution to the overall emission upon excitation with light of $\lambda_{exc} \geq 341$ nm could not be observed with our experimental set-up.

Derivatization of the silicon surface with MPTS modifies the spectrum and/or the relative intensity of the emitter peaks. The emitters PSi2 and PSi-SH2 show, within the experimental error, coincident excitation and emission spectra, as well as coincident decay times. Because of their matching PL properties, these emitters are attributed to the same species. A similar observation applies for PSi1 and PSi-SH1 emitters. Therefore the PL of these species is not modified by surface derivatization, though their relative contribution to the overall emission is inverted after MPTS grafting.

On the other hand, though PSiSH3 and PSi3 absorb and emit in the same wavelength range, their different emission spectra and decay times suggest that they are originating from different emitting species. The results clearly show that PSiSH3 is formed as a consequence of MPTS grafting onto the particles' surface. On the other hand, similar excitation–emission spectra in un-oxidized Si–NP toluene suspensions were assigned to the presence of particle aggregates.[14]

Molecular oxygen is able to quench the observed luminescence intensity of both, PSi-NP and PSi-NP-SH toluene suspensions. The spectrum shape is not perturbed by the presence of O_2. Observed emission quantum yields, Φ_{em}, and luminescence decay times, τ, in argon-bubbled and oxygen-saturated toluene suspensions are depicted in Table 1.

Table 1 Emission quantum yields (Φ_{em}) and luminescence decay times (τ) obtained by 341 and 388 nm excitation measured for PSi-NP and PSi-NP-SH under O_2– and Ar– saturated toluene suspensions at room temperature

	Φ_{em} λ_{exc}. 366 nm		$\tau_{341\ exc}$/ns		$\tau_{388\ exc}$/ns	
[O₂]/mM	0.0	2.3	0.0	2.3	0.0	2.3
PSi-NP-SH	0.30	0.25	3.35 ± 0.04	1.40 ± 0.03	—	1.8 ± 0.1
			43.6 ± 0.3	8.5 ± 0.2		
PSi-NP		0.053	0.036	27.5 ± 0.3	8.8 ± 0.2	5.0 ± 0.3 3 ± 1

Si-NP and Si-NP-SH

Toluene suspensions of aged Si-NPs show an excitation–emission matrix which, according to a bilinear analysis, is due to the contribution of three emitting species, namely Si-NP1, Si-NP2 and Si-NP3 with (λ_{exc}./nm, λ_{em}./nm): (310, 370), (350, 385), (375, 430), see the line plot in Fig. 8. After derivatization of Si-NPs with MPTS (Si-NP-SH), the excitation–emission matrix shows the contribution of emitting species with (λ_{exc}./nm, λ_{em}./nm): (335, 385) and (375, 435), namely SiNP-SH2 and SiNP-SH3, respectively, in agreement with the emission–excitation spectrum of Si-NP2 and Si-NP3 species. In fact, MPTS grafting leads to an increase in the emission intensity of the (375, 430) nm band, as shown in the symbol plot of Fig. 8. For the Si-NP and Si-NP-SH excitation–emission matrix, see ESI, Fig. 2.†

The emission of air-saturated toluene suspensions of Si-NP and Si-NP-SH, obtained upon excitation at 341 nm, yields traces that could be well fitted to a bi-exponential function with decay times of: 1.7 ± 0.8 and 14 ± 4 ns, and 2.5 ± 0.6 and 10.8 ± 0.6 ns, respectively. The short-lived components contribute to the emission with the spectrum coincident with those expected for species Si-NP3.

Anisotropy experiments

Time-domain anisotropy experiments were performed for bare and silicon modified nanoparticles suspended in toluene. The measured anisotropy time profiles follow a single exponential with $r(t) = r_o \times \exp(-t/\theta)$ (see Fig. 3, ESI†) from which the
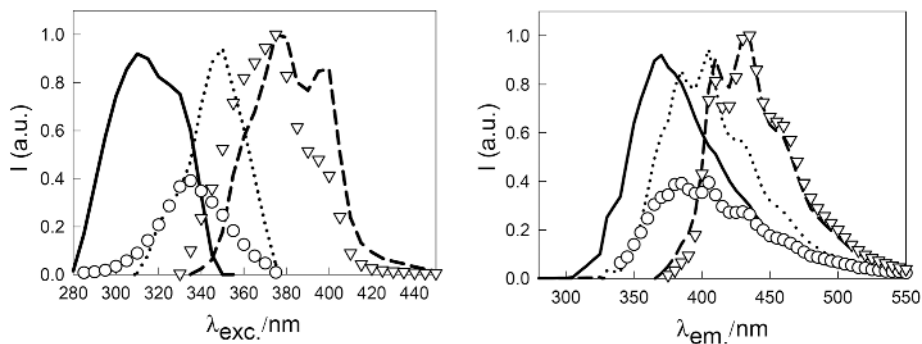
This journal is © The Royal Society of Chemistry and Owner Societies 2013

Photochem. Photobiol. Sci., 2013, **12**, 1658–1665 | **1661**

Fig. 8 Excitation (left figure) and emission (right figure) spectrum obtained from the bilinear regression analysis of Si-NP (line plot) and Si-NP-SH (symbol plot) toluene suspension excitation–emission matrices. The assigned species are Si-NP1 (full line), Si-NP2 (dotted line), Si-NP3 (dashed line), SiNP-SH2 (O) and SiNP-SH3 (▽), respectively. The intensity was normalized taking the maximum value $I = 1$ for the species Si–NP3 and SiNP-SH3.

rotational correlation times θ and the anisotropy at time zero r_o are determined. The observation of a single exponential is compatible with emission mainly originating from a population of particles with identical three perpendicular rotational axes. The time of Brownian rotation of a molecule, θ, gives information on the hydrodynamic radius (R) by the Stokes–Einstein–Debye relation.[22] On the other hand, r_o is related to the relative orientation of the absorption and emission dipole moments of the particles.

The dependence of θ on the volume (V) for spherical particles, given by the simple hydrodynamic theory of the rotational diffusion, is $\theta = \eta V/k_B T$, where k_B is the Boltzmann constant and η is the shear viscosity of the solvent.

The time-domain anisotropy experiments with toluene suspensions of PSi-NP and PSi-NP-SH were performed exciting at 341 nm and detecting the emission at 380 nm. Under these conditions, mainly information of species PSi2 and PSi-SH2 is obtained. Within the experimental error, an average value $r_0 = 0.383 \pm 0.006$ and $r_0 = 0.399 \pm 0.004$ is obtained for PSi-NP and PSi-NP-SH, respectively. Taking the value 554.2 μPas for the viscosity of toluene at 298 K,[23] the estimated average hydrodynamic diameter $\langle D \rangle = (2.2 \pm 0.4)$ nm is retrieved from the rotational correlation times of (0.78 ± 0.05) and (0.83 ± 0.02) ns for PSi-NP and PSi-NP-SH, respectively.

Both particles show, within the experimental error, the same r_0 which therefore indicates that the dipole orientation of the excited states leading to the observed luminescence does not depend on surface coverage. R_0 experimental data are very close to 0.4, the value accepted for fluorophores with collinear absorption and emission transition moments.

Excitation at 341 nm, of air-saturated toluene suspensions of Si-NP and Si-NP-SH nanoparticles, yields information mainly on species Si-NP3.[14] An average hydrodynamic diameter $\langle D \rangle$ of (2 ± 1) nm is obtained for this species. The measured size of amorphous Si-NPs was reported to correlate with theoretical data of the band gap energy.[14]

The mean band gap energy of the particles may be calculated from the excitation spectrum threshold of each individual species, as demonstrated in the literature.[14,24] For PSi-NP

emitting species, there is coincidence between the energy gap values and the emission maxima suggesting that the excitation and the emission are mainly originating from the same transition, as expected for a quantum confined emission. On the assumption that the observed luminescence is controlled by quantum confinement, the expected particle size for each species can be estimated from theoretical correlations of the band gap energy with size reported for crystalline silicon nanoparticles.[25] Taking the maximum emission wavelength of 385 and 360 nm for PSi2 and PSi1, respectively, the correlations predict, within the experimental error, an average particle size $\langle D \rangle = 1.4 \pm 0.1$ nm.

PSi-NP and PSi-NP-SH particles show a particle diameter of (2.2 ± 0.4) nm by time domain anisotropy, (1.6 ± 0.5) nm by STM and (1.7 ± 0.3) nm by AFM microscopy, close to those found by theoretical correlation.

During the silanization reaction with MPTS on partially oxidized silicon nanoparticles, $Si-O-Si-(CH_2)_3-SH$ structures are formed on the surface. These nanoparticles retain the luminescence, changing the PL intensity of the different contributing emitters to the excitation–emission matrix. Silanized particles synthesized by the two different methods show similar PL characteristics: an increase in the PL intensity emission at wavelengths from 400 to 430 nm and a PL quenching of peaks at shorter wavelengths.

Compared to silicon nanoparticles composed of a silicon core and a SiO_x shell (TDSiNPs),[14] PSi-SH3 and SiNP-SH3 have the same excitation–emission PL spectra as the species with $(\lambda_{exc}/nm, \lambda_{em}/nm)$: (375, 435) (Fig. 9), and similar decay time (τ).

Doubly bonded oxygen at the surface of small Si clusters has been predicted to introduce defect states in the gap that permit radiative electron–hole recombination at energies smaller than the cluster band gap.[26–28] In TDSiNP nanoparticles, the $(\lambda_{exc}/nm, \lambda_{em}/nm)$: (375, 435) transition is reported to be associated with the presence of surface SiO_x. Silanization also introduces a SiO_x surface layer leading to a similar transition, however, the presence of doubly bonded oxygen in not expected in these systems.

1662 | *Photochem. Photobiol. Sci.*, 2013, **12**, 1658–1665

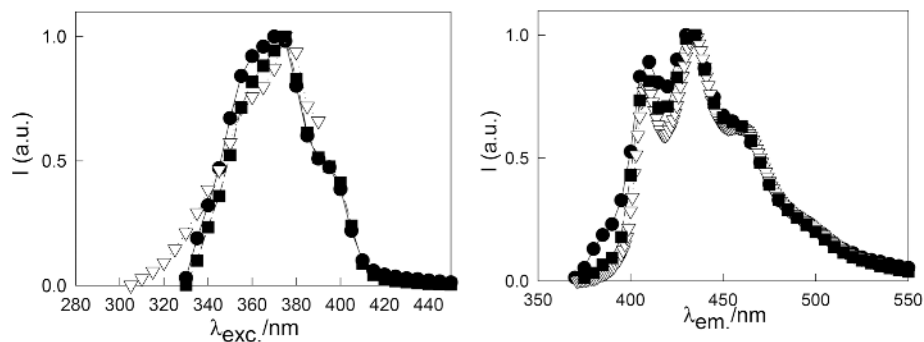This journal is © The Royal Society of Chemistry and Owner Societies 2013

Fig. 9 Normalized excitation (left figure) and emission (right figure) spectrum obtained from the bilinear regression analysis of the Si-NP-SH toluene suspension excitation–emission matrix corresponding to TDSiNP (▽),[14] SiNP-SH3 (■) and PSi-SH3 (●). The intensity was normalized taking the maximum value $I = 1$ in each case.

3. Experimental

Materials and methods

Materials. The organic 3-mercaptopropyltrimethoxysilane (Aldrich) was used as received. Toluene (99.7%, H_2O 0.005%), cyclohexane (99%), methanol (99.8%), HF (48%), $SiCl_4$ (99%), ethyl ether (p.a. 99.9%), $LiAlH_4$ (95%), and tetraoctylammonium bromide (98%), were purchased from Sigma-Aldrich and employed without further purification. When required, toluene and methanol were dried over molecular sieves for 24 hours.

Distilled water (>18 MΩ cm, <20 ppb organic carbon) was obtained from a Millipore (Bedford, MA) system. Argon gas (4 bands quality) was from La Oxígena S.A., Argentina.

Silicon nanoparticle synthesis. Synthesized silicon nanoparticles were obtained in the laboratory by two different approaches.

Colloidal particles of porous silicon were obtained by electrochemical etching of p-type crystalline silicon wafers (resistivity between 1.0 and 10.0 Ω cm).[9] After anodization, the particles were released by ultrasound in toluene. The resulting suspension was filtered with 100 nm PVDF Durapore® VVPP Membrane Filters (Millipore) keeping the solid residue. The porous solid was suspended in a 3% HF methanol solution, sonicated and stored in the dark to break up and etch agglomerates.[29] The particle dispersion became less turbid with time until it became completely clear after 24 h. The clear, well-dispersed particle suspension was treated with cyclohexane to extract the resulting hydrophobic particles to the organic phase. The solvent was evaporated and the silicon dispersed in toluene for characterization and further functionalization reactions. These particles will be referred to as PSi-NPs.

The second approach (bottom-up method) involved an adaptation of the wet chemical method reported by Rosso-Vasic.[14,15] The synthesis was performed in a two-necked glass flask with one entrance for the continuous bubbling with argon gas and the other for the introduction of reactants and gas vent. In a first step, 16 mL of dry toluene and 6.3 g of tetraoctylammonium bromide (TOAB) were introduced and sonicated for 20 minutes to form TOAB reversed micelles. In a second step, 0.6 mL of $SiCl_4$ was added and sonicated for 20 minutes. Reduction of $SiCl_4$ by 10 M $LiAlH_4$ in ethyl ether was performed under constant sonication during 30 minutes. Any excess of $LiAlH_4$ is consumed by addition of 30 mL of methanol. The suspension was taken to dryness on a rotary evaporator and re-suspended in cyclohexane to eliminate TOAB by precipitation, cyclohexane was then evaporated and NPs re-suspended in toluene. These particles will be referred to as Si-NPs.

Surface-modification procedure. Surface derivatization was performed employing silane as a coupling agent to terminal Si–OH groups.[15,30] Surface terminated H–Si and Cl–Si particles, as obtained in PSi-NPs and Si-NPs, respectively, are unstable towards O_2. Therefore, the as-prepared silicon nanoparticles were oxidized during storage of their toluene suspensions under air-saturation for several days,[14] as confirmed by the appearance of a broad band near 3600 cm^{-1} in the FTIR spectrum which corresponds to O–H stretching vibration. XPS spectra also indicate surface oxidation (see below).

The suspended surface-oxidized PSi-NP and Si-NP in toluene were treated with MPTS and stirred for 24 hours.[15] An excess of organosilane and TOAB were removed by membrane dialysis until the outer membrane solution was negative to the test for mercaptyl groups. Modified samples were namely: PSi-NP-SH and Si-NP-SH, which are referred to as treated porous silicon colloids and bottom-up silicon nanoparticles, respectively.

Toluene was used as a solvent of the silicon nanoparticle suspensions in all the experiments.

Characterization techniques

TEM. Images were acquired using a Philips CM200 UT microscope (point to point resolution 0.19 nm) operated at 200 kV and room temperature. Samples were prepared by placing drops of the aqueous PSi-NP suspensions on a carbon grid followed by drying at room temperature. Images were analyzed employing the Image Tool 3.0 software (Health Science Center of the University of Texas, San Antonio, USA). Particle diameters were determined assuming that the particle area obtained from the TEM images is the projection of a spherical particle.

STM. A flame-annealed Au(111) substrate was placed in a solution (toluene) with thiol-terminated silicon nanoparticles for 15 hours. These particles were attached to an Au substrate by an Au–S bond.

Microscopy imaging was done in air in the constant current mode with a Nanoscope IIIa microscope from Veeco Instruments (Santa Barbara, CA) with commercial Pt–Ir tips. Typical tunneling currents, bias voltages, and scan rates were 1 nA, 100 mV, and 1–5 Hz, respectively.

AFM. Tapping-mode AFM (Nanoscope IIIa, Digital Veeco Instruments, Santa Barbara, CA) was used to characterize the substrates using RTESP Arrow-NCR-50 Nano World (cantilever resonance frequency: 357 kHz, force constant 20–80 N m^{-1}; tip radius 5–10 nm). The sample was attached to a mica substrate and dried under nitrogen.

FTIR. Spectra in the range from 4000 to 400 cm^{-1} were recorded on a Thermo Scientific, Nicolet 8700 apparatus with a Smart Multi Bounce HATR, ZnSe 45° plate as accessory.

Raman spectroscopy measurements. The Raman spectra were recorded with a Bruker IFS 66 FTIR spectrophotometer provided with the NIR Raman attachment.

XPS. The spectra were obtained under UHV with an XR50 Specs GmbH spectrometer with Mg K(R) as the excitation source and a PHOIBOS 100 half-sphere energy analyzer. Calibration was performed with Au4f 7/2, C2p and Cu2p 3/2 with binding energies of 84.00, 285.00 and 933.67 eV, respectively.

Room temperature luminescence. Steady-state luminescence measurements were performed with a Perkin-Elmer LS-50B spectrometer equipped with a Xe lamp as an excitation source, a monochromator for selecting the excitation and emission wavelengths (both with a 5 nm band pass gap), and a red sensitive R928 p.m. as a detector. All spectra were corrected for the wavelength-dependent sensitivity of the detector and the source by recording reference data simultaneously. Additionally, emission spectra were corrected for Raman scattering by using the solvent emission spectrum.

Suspensions of bare and surface modified silicon nanoparticles were excited in the range of 250–450 nm. The emission spectra were collected in the 250–550 nm range.

To estimate the quantum yield of the synthesized Si nanoparticles, PL emission spectra were collected at various excitation wavelengths. Identical measurements (excitation conditions, lamp energy, and spectrometer band-pass) were performed on 9,10-diphenylanthracene in cyclohexane, which emits between 400 and 500 nm with a known efficiency of 95% at 366 nm excitation.[31] A comparison of the ratios between the area of the emission spectrum and the absorbance at a given excitation wavelength yields Φ, as depicted in eqn (1).[32]

$$\Phi = \Phi_R \times \frac{I}{I_R} \times \frac{1 - 10^{-A_R}}{1 - 10^{-A}} \times \left(\frac{n}{n_R}\right)^2 \qquad (1)$$

where I is the total emission intensity, A is the absorbance at a given excitation wavelength, n is the solvent refractive index, and suffix R stands for the reference.

Luminescence lifetime and anisotropy. Luminescence lifetime measurements were performed with a JOBIN-YVON SPEX FLUOROLOG FL3-11 with lifetime TCSPC (time correlated single photon counting) with LED excitation at 341 and 388 nm.

Time Resolved Emission Spectroscopy (TRES) was performed and results fitted to an exponential model until optimal values of Chi square, residuals, and standard deviation parameters were attained. The emission spectrum associated with each lifetime may be obtained taking the contribution of each decay lifetime to the overall emission at a given wavelength, weighted by the emission intensity at the emission maximum.

In order to evaluate the participation of molecular dissolved oxygen in luminescence lifetime of nanoparticle suspensions, samples were deoxygenated by sparking with argon gas for 20 min.

Bilinear regression analysis. For each excitation wavelength of the particle suspension an emission spectrum is obtained. For a pure substance existing in a unique form, the luminescence spectrum is invariant, remaining the same independent of the excitation wavelength. For low fluorophore absorbance (<0.05), the steady state emission intensity at a given emission wavelength ($I(\lambda_m)$) is proportional to the absorption coefficient of the fluorophore at a given excitation wavelength ($\varepsilon(\lambda_x)$), the concentration of the fluorophore, and the factor $F(\lambda_m)$ reflecting the distribution of the probability of the various transitions from the lowest vibrational level of the first electronic excited level to the various vibrational levels of the ground state.[33] A bilinear regression analysis taking advantage of the linearity of $I(\lambda_m)$ with both, $\varepsilon(\lambda_x)$ and $F(\lambda_m)$, was applied to the experimental emission matrix in order to retrieve information on the minimum number of species and on their relative emission and absorption spectra. Using the running indexes x and m for the excitation and emission wavelengths, respectively, in a matrix form $[i_{xm}] = [\varepsilon_{xj}] \cdot [f_{jm}]$, where $[i_{xm}]$, $[\varepsilon_{xj}]$ and $[\mathbf{f}_{jm}]$ represent the emission intensity, absorption coefficients, and $F(\lambda_m)$ matrices, respectively. The procedure is based on the alternating calculus of the matrices $[\varepsilon_{xj}]$ and $[f_{jm}]$ by multiple linear regression iteratively until convergence is achieved when a least-squares condition is applied in order to minimize the elements of an error matrix. From the error matrix, a corrected emission intensity matrix, $[i_{xm}{}^c]$, is obtained. The number of species is selected as the minimum that shows a reasonable approximation between $[i_{xm}{}^c]$ and $[i_{xm}]$.[34]

4. Conclusion

In PSi-NP-SH and Si-NP-SH particles, the Si–O–Si structure is stabilized on the surface after derivatization with MPTS. These defect levels at the silicon surface play an important role in the emission process and are proposed to be responsible for the excitation emission red-shifted peak at (375, 435) nm. In conclusion, no matter the synthesis method, size, and crystalline structure of the particles, the surface layer network of Si–O–Si

1664 | *Photochem. Photobiol. Sci.*, 2013, **12**, 1658–1665

This journal is © The Royal Society of Chemistry and Owner Societies 2013

contributes to the overall emission of silicon nanoparticles with a characteristic emission–excitation spectrum in the visible range.

The new insights obtained here improve our fundamental understanding of the red-shifted PL band in silicon nanoparticles due to silanization. These results are important for synthesis and application of semiconductor nanoparticles where surface defects are capable of undergoing energy transfer to adsorbed molecules, as reported by Llansola Portoles et al., 2009 and 2010.[9,10]

Acknowledgements

References

1 L. T. Canham, *Adv. Mater.*, 1995, **7**, 1033–1037.

2 M. Thust, M. J. Schoning, S. Frohnhoff, R. Arens-Fisher, P. Kordos and H. Luth, *Meas. Sci. Technol.*, 1996, **7**, 26–29.

3 L. T. Canham, *Appl. Phys. Lett.*, 1990, **57**, 1046–1048.

4 R. Jugdaohsingh and J. Nutr, *Health Aging*, 2007, **11**, 99–110.

5 Y. C. Yoo, S. K. Lee, J. Y. Yang, S. W. In, K. W. Kima, K. H. Chung, M. G. Chung and S. Y. Choung, *J. Health Sci.*, 2002, **48**, 186–194.

6 S. C. Bayliss, L. D. Buckberry, P. J. Harris and M. Tobin, *J. Porous Mater.*, 2000, **7**, 191–195.

7 S. P. Low, N. H. Voelcker, L. T. Canham and K. A. Williams, *Biomaterials*, 2009, **30**, 2873–2880.

8 C. B. Murray, D. J. Norris and M. G. Bawendi, *J. Am. Chem. Soc.*, 1993, **115**(19), 8706–8715.

9 M. J. Llansola Portoles, F. Rodriguez Nieto, D. B. Soria, J. I. Amalvy, P. J. Peruzzo, D. O. Martire, M. Kotler, O. Holub and M. C. Gonzalez, *J. Phys. Chem. C*, 2009, **113**, 13694–13702.

10 M. J. Llansola Portoles, P. M. David Gara, M. L. Kotler, S. Bertolotti, E. San Roman, H. B. Rodríguez and M. C. Gonzalez, *Langmuir*, 2010, **26**, 10953–10960.

11 L. Xu, L. Jianhu, H. Lan, G. Ning, Z. Haiqian and L. Juzheng, *Appl. Surf. Sci.*, 2003, **211**, 184–188.

12 S. T. McBain, H. H. P. Yiu and J. Dobson, *Int. J. Nanomed.*, 2008, **3**, 169–180.

13 P. Caregnato, M. D. E. Forbes, D. B. Soria, D. O. Martire and M. C. Gonzalez, *J. Phys. Chem. C*, 2010, **114**, 5080–5087.

14 M. J. Llansola Portoles, R. Pis Diez, M. L. Dell'Arciprete, P. Caregnato, J. J. Romero, D. O. Martire, O. Azaroni, M. Ceollin and M. C. Gonzalez, *J. Phys. Chem.*, 2012, **116**, 11315–11325.

15 M. Rosso-Vasic, E. Spruijt, B. V. Lagen, L. D. Cola and H. Zuilhof, *Small*, 2008, **4**, 1835–1841.

16 J. Coates, in *Interpretation of Infrared Spectra, A Practical Approach, Encyclopedia of Analytical Chemistry*, ed. R. A. Meyers, John Wiley & Sons Ltd, 2000, pp. 10815–10837.

17 S. Kinugasa, K. Tanabe and T. Tamura, *Spectral Database for Organic Compounds, SDBS*, National Institute of Advanced Industrial Science and Technology (AIST), Japan, 2009. Available online at: http://riodb01.ibase.aist.go.jp/sdbs/cgi-bin/cre_index.cgi?lang=eng

18 F. Zhou, W. Liu, M. Chen and D. C. Sun, *Chem. Commun.*, 2001, 2446–2447.

19 M. C. Ferrara, L. Mirenghi, A. Mevoli and L. Tapfer, *Nanotechnology*, 2008, **19**, 365706–365715.

20 L. Pasquali, F. Terzi, R. Seeber, S. Nannarone, D. Datta, C. Dablemont, H. Hamoudi, M. Canepa and V. A. Esaulov, *Langmuir*, 2011, **27**, 4713–4720.

21 Z. Mekhalif, J. Riga, J.-J. Pireaux and J. Delhalle, *Langmuir*, 1997, **13**, 2285–2290.

22 P. Debye, *Polar Molecules*. The Chemical Catalogue Company, New York, 1929, pp. 77–108.

23 D. R. Lide, *Handbook of Chemistry and Physics*, CRC Press. Inc., Boca Raton, 2009.

24 A. Saren, S. Kuznetsov, V. Pikulev, Y. Gardin and V. Gurtov, *Tech. Phys. Lett.*, 2001, **27**, 328–330.

25 B. Delley and E. F. Steigmeier, *Appl. Phys. Lett.*, 1995, **67**, 2370–2372.

26 R. Mohan Sankaran, D. Holunga, R. C. Flagan and K. P. Giapis, *Nano Lett.*, 2005, **5**(3), 537–541.

27 E. V. Rogozhina, D. A. Eckhoff, E. Gratton and P. V. Braun, *J. Mater. Chem.*, 2006, **16**, 1421–1430.

28 V. Švrček, T. Sasaki, Y. Shimizu and N. Koshizaki, *Appl. Phys. Lett.*, 2006, **89**, 213113–213115.

29 X. Li, Y. He and M. T. Swihart, *Langmuir*, 2004, **20**, 4720–4727.

30 X. Li, Y. He and M. T. Swihart, *Langmuir*, 2004, **20**, 4720–4727.

31 S. Hamal and F. Hirayama, *J. Phys. Chem.*, 1983, **87**, 83–89.

32 J. R. Lakowicz, *Principles of Fluorescence Spectroscopy*, Springer Science Business Media, New York, 3 edn, 2006.

33 B. Valeur, *Molecular Fluorescence. Principles and Applications*, Wiley-VCH, Weinheim, Germany, 2002.

34 M. C. Gonzalez and E. San Roman, *J. Phys. Chem.*, 1989, **93**, 3536–3540.

This journal is © The Royal Society of Chemistry and Owner Societies 2013

Photochem. Photobiol. Sci., 2013, **12**, 1658–1665 | **1665**